Motion Algorithm for Large-Displacement Driving Simulator

L. D. REID AND P. R. GRANT

Renewed interest in developing driving simulators with large motion amplitudes has engendered simulator motion drive algorithms and computer software capable of predicting the performance of such devices for design purposes. One such computer package is described. The hardware is assumed to consist of an unrestricted turntable on top of a hexapod motion platform carried by a large-amplitude *x-y* carriage. Algorithms are included to represent the motion-drive washout algorithms and the physical motion of the simulator. Routines are developed to split the six linear and angular motions among the three principal hardware subsystems. The presence of an unrestricted turntable has resulted in the need to develop a new tilt-coordination algorithm to simulate sustained accelerations. By selecting a Euler angle set specifically suited to the present geometry, a considerable simplification of the washout algorithm has been achieved. Potential problems with algorithm stability and crosstalk are pointed out, and guidelines on how to avoid them are provided. Several typical car maneuvers are employed to demonstrate the features of the motion algorithm and the benefits and limitations of the hardware configuration. These maneuvers include an entry and steady turn, braking, and a single lane change. The effects of including and deleting the turntable and the *x-y* carriage are studied. The results are described in terms of the amounts of hardware travel used and the fidelity of the motion cues provided to the driver.

Recent interest in high-performance driving simulators has led to the production of several facilities capable of large amplitude motion such as the Daimler-Benz system (*1*) and the Swedish VTI system (*2*). In addition, conceptual designs have been proposed with 9 degrees of freedom (*3*), and the National Advanced Driving Simulator (NADS) (*4*) is gaining momentum in the United States.

To assess the problems involved with operating recently proposed large-amplitude simulator motion-drive systems and the cost/benefits associated with the increased size, a software package has been developed that can produce a computer simulation of both the motion of the physical hardware and the performance of the motion-drive algorithms that must be used to interface the vehicle equations of motion and the hardware (*5,6*).

Before the software could be created it was necessary to specify the general characteristics of the lage-amplitude motion-base hardware. The configuration selected was based on a standard flight simulator hexapod motion system (supported by six hydraulic actuators) as is the Daimler-Benz simulator. This was taken to be mounted on a large-amplitude *x-y* carriage producing motions in the horizontal plane. Finally, an unrestricted turntable was mounted on the hexapod's upper payload platform and the vehicle cab affixed to the turntable.

This paper will not deal with the details of the mechanical design or with the dynamic response characteristics of the hardware. It will be assumed that the software and hardware are well matched so that each hardware subsystem has a high bandwidth relative to the motion command signals it receives from the motion-drive software. It will also be assumed that the hexapod and the turntable both have the same high-bandwidth properties due to the modest mass they must support. The *x-y* carriage, on the other hand, is assumed to be a more massive low-frequency device (see Figure 1). All mechanical systems are assumed to have unity transfer functions over the frequency range of their input command signals.

The goal of the classical washout algorithm used herein is to match as closely as possible the angular velocity $\underset{\rightarrow}{\omega}$ and specific force $\underset{\rightarrow}{f}$ at a particular reference point in the actual vehicle (the origin of F_A) and the simulated vehicle (the origin of F_S) (*7,8*). Here, specific force at a point is defined to be

$$\underset{\rightarrow}{f} = \underset{\rightarrow}{a} - \underset{\rightarrow}{g} \tag{1}$$

where $\underset{\rightarrow}{a}$ is the inertial acceleration of the point and $\underset{\rightarrow}{g}$ is the acceleration due to gravity. The algorithm is intended to produce the desired motion cues mentioned while restricting the motion of the hardware to remain within its physical limitations. Without going into the details to be covered later in this paper, Figures 2 and 3 can be used to illustrate the essential features of the classical washout algorithm. The inputs to the algorithm are $\underline{\omega}_{AA}$ and $\underline{f}_{AA}$, the computed angular velocity and specific force at the selected reference point in the vehicle being simulated. The outputs from the algorithm are ℓ_{3i}, $\underline{C}_I$, and ψ_{TT}, the input commands to the motion-base hardware. Consider $\underline{\omega}_{AA}$: it is first scaled and limited to reduce the demands on the motion system. It is then converted to Euler angles, which are fed through high-pass filters to remove low-frequency signals that tend to drive the motion system into its travel limits. These Euler angles are then used to help generate the hardware drive signals and to produce transformation matrices at various points in the algorithm. Now consider $\underline{f}_{AA}$: after being scaled and limited, it is transformed into earth frame components and high-pass-filtered and double-integrated to produce linear displacement commands. As before, the removal of low-frequency signals is the goal of this process. With most of the computed low-frequency motions removed by the high-pass filters, a special effect has been developed to represent sustained accelerations in the *xy* plane

L. D. Reid, Institute for Aerospace Studies, University of Toronto, 4925 Dufferin Street, Downsview, Ontario, Canada M3H 5T6. P. R. Grant, Aerospace Engineering and Research Consultants Limited, 4925 Dufferin Street, Downsview, Ontario, Canada M3H 5T6.

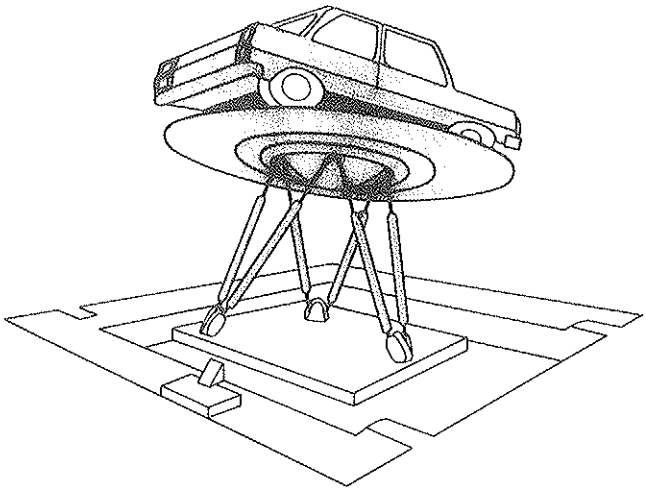

FIGURE 1 Hardware configuration.

of the vehicle axis system. It is called tilt-coordination, and it makes use of Equation 1. When $\underline{a}$ is 0, $\underline{f}$ can still be simulated by $\underline{g}$. For example, the sensation of forward sustained acceleration in the simulator cab can be created by placing the cab in a pitched-up attitude. The driver's vestibular system and the sensation of the seat pressing against his back both register cues that the driver would experience if he or she were indeed accelerating forward. In Figures 2 and 3 the tilt-coordination is created by passing a modified version of $\underline{f}_{AA}$ (namely $\underline{f1}$) first through a low-pass filter to pick up its low-frequency component and then creating an increment to the simulator's Euler angles that approximates the desired tilt.

REFERENCE FRAMES

Frame F_H

The hexapod frame F_H is located with its origin on the payload platform at the point at which the turntable's axis of rotation meets the platform. The x-axis points forward and the z-axis downward. The xy plane is parallel to the payload platform. It is assumed that the axis of rotation of the turntable is coincident with the z-axis and that the floor of the simulator cab is also parallel to the xy plane.

Frame F_S

The simulator frame F_S has its origin in the simulator cab at a point selected to suit the requirements of the simulation. It is attached to the cab with its x-axis pointing forward and its z-axis parallel to the z-axis of F_H.

Frame F_P

Frame F_P is fixed to the simulator driver's head with its origin midway between the driver's left and right vestibular systems. The x-axis points forward and the z-axis downward along the spine. In this study it will be assumed that F_P is parallel to F_S.

Frame F_A

The car reference frame F_A has its origin at the same relative cab location as the simulator reference frame F_S. Frame F_A

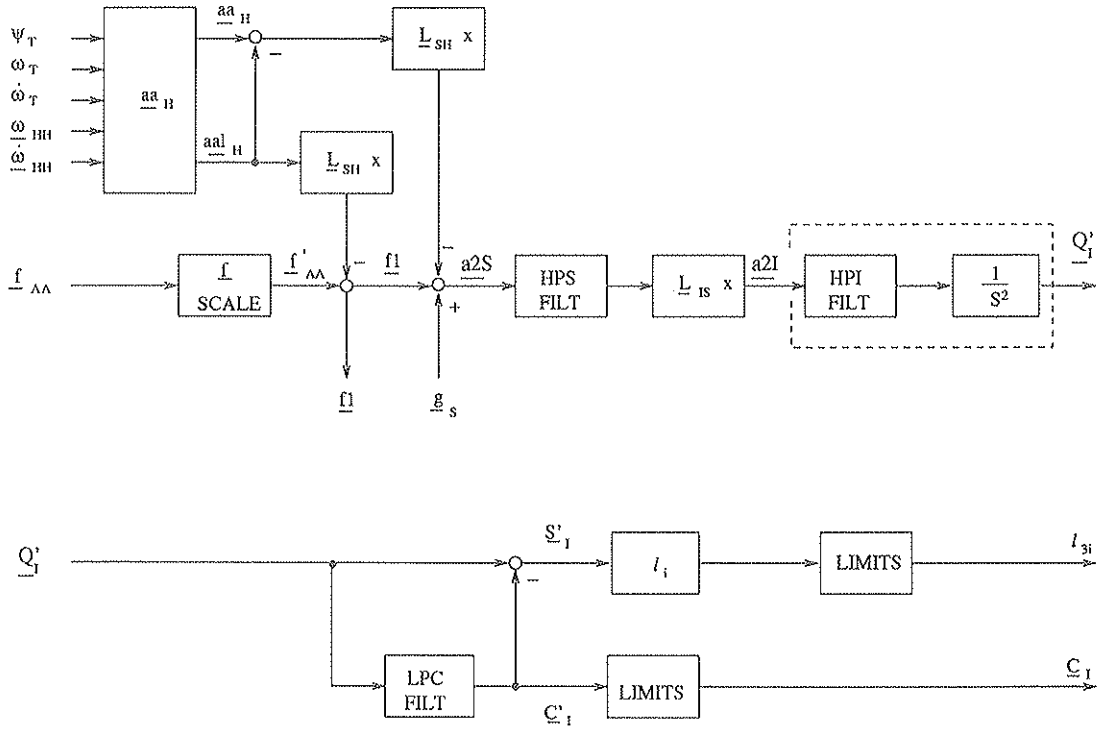

FIGURE 2 Classical algorithm: linear motion.

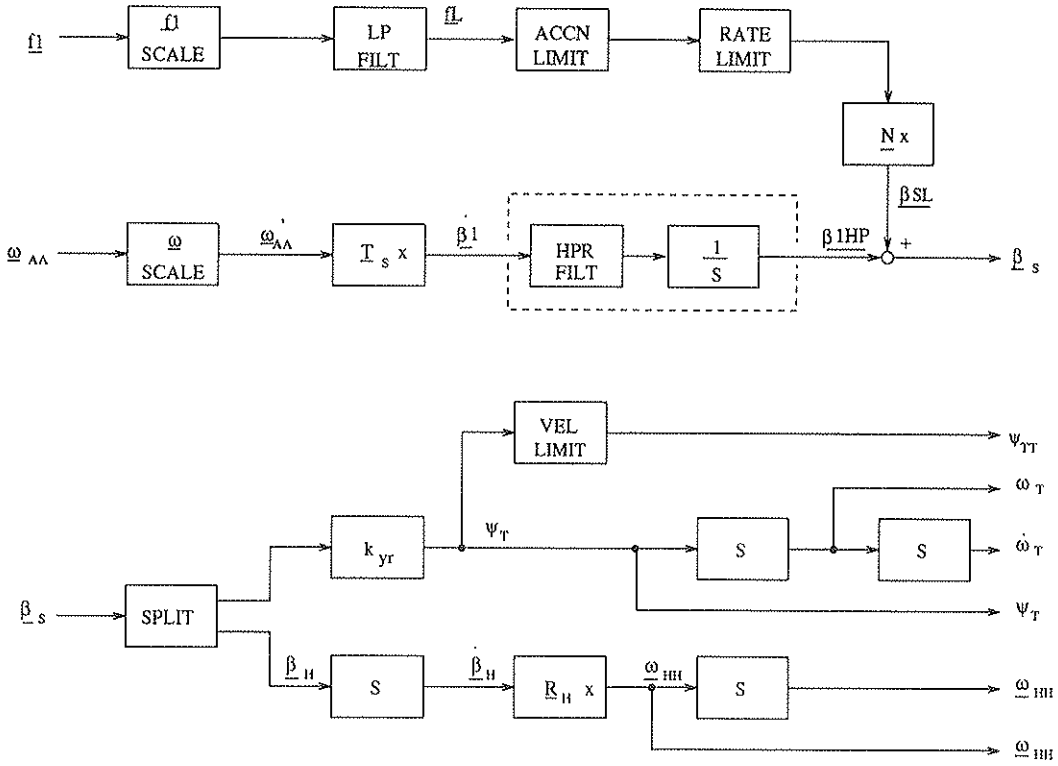

FIGURE 3 Classical algorithm: angular motion.

has the same orientation with respect to the cab as the simulator frame F_S.

Frame F_I

The inertial frame F_I is earth-fixed with its z-axis aligned with the gravity vector $\underrightarrow{g}$. The location of its origin and the orientation of its x-axis are selected to suit the problem under study.

Frame F_V

The x-y carriage frame has its origin fixed to the centroid of the hexapod's lower platform bearing attachment points. It is parallel to F_I and is translated by the x-y carriage.

EULER ANGLES AND TRANSFORMATION MATRICES

With the F_H and F_S frames related as described, it is found that the formulations involving the calculation of angular rates and Euler angles are simplified if a nonstandard set of Euler angles is employed. In the present development the order of rotation when applying Euler angles will be roll (ϕ), pitch (θ), then yaw (ψ). In general, the three Euler angles will be represented by

$$\underline{\beta} = [\phi\ \theta\ \psi]^T \tag{2}$$

If the turntable angles relative to the hexapod be ψ_T, then it follows that

$$\underline{\beta}_S = \underline{\beta}_H + [0\ 0\ \psi_T]^T \tag{3}$$

The transformation matrices based on the present nonstandard Euler angles are (for a general frame F_B)

$$\underline{L}_{IB} = \begin{bmatrix} \cos\theta\cos\psi & -\cos\theta\sin\psi & \sin\theta \\ \cos\phi\sin\psi & \cos\phi\cos\psi & -\sin\phi\cos\theta \\ +\sin\phi\sin\theta\cos\psi & -\sin\phi\sin\theta\sin\psi & \\ \sin\phi\sin\psi & \sin\phi\cos\psi & \cos\phi\cos\theta \\ -\cos\phi\sin\theta\cos\psi & +\cos\phi\sin\theta\sin\psi & \end{bmatrix}_B$$

$$= \underline{L}_{BI}^T \tag{4}$$

where $[\phi\ \theta\ \psi]_B^T$ are the Euler angles of F_B relative to F_I and where in general for any vector $\underrightarrow{V}$

$$\underline{V}_I = \underline{L}_{IB}\,\underline{V}_B \tag{5}$$

$$\underline{L}_{SH} = \begin{bmatrix} \cos\psi_T & \sin\psi_T & 0 \\ -\sin\psi_T & \cos\psi_T & 0 \\ 0 & 0 & 1 \end{bmatrix}$$

$$= \underline{L}_{HS}^T \tag{6}$$

$$\underline{\omega}_{BB} = \underline{R}_B\,\dot{\underline{\beta}}_B \tag{7}$$

$$\dot{\underline{\beta}}_B = \underline{T}_B\,\underline{\omega}_{BB} \tag{8}$$

$$\underline{R}_B = \begin{bmatrix} \cos\theta\cos\psi & \sin\psi & 0 \\ -\cos\theta\sin\psi & \cos\psi & 0 \\ \sin\theta & 0 & 1 \end{bmatrix}_B \tag{9}$$

$$\underline{T}_B = \begin{bmatrix} \sec\theta\cos\psi & -\sec\theta\sin\psi & 0 \\ \sin\psi & \cos\psi & 0 \\ -\tan\theta\cos\psi & \tan\theta\sin\psi & 1 \end{bmatrix}_B \tag{10}$$

SYSTEM GEOMETRY

The linear displacement geometry including the ith hexapod actuator is shown in Figure 4. $\vec{Q}$ gives the location of the origin of F_H relative to the origin of F_I, and $\vec{C}$ the location of the origin of F_V relative to the origin of F_I. The displacement $\vec{C}$ is generated by motion of the x-y carriage. As shown in the figure, $\vec{S}$ gives the location of the origin of F_H relative to the origin of F_V so that

$$\vec{Q} = \vec{C} + \vec{S} \tag{11}$$

In the figure $\vec{A}_i$ and $\vec{B}_i$ locate the upper and lower attachment points of the hexapod's ith actuator, and $\vec{\ell}_i$ represents the ith actuator. Thus, $\vec{\ell}_i$ expressed in F_I components becomes

$$\underline{\ell}_{iI} = \underline{L}_{IH}\,\underline{A}_{iH} - \underline{B}_{iI} + \underline{S}_I \tag{12}$$

where $\underline{A}_{iH}$ and $\underline{B}_{iI}$ are constants for given hexapod geometry. The actuator length command signal relative to its neutral position is given by

$$\ell_i = (\underline{\ell}_{iI}^T\,\underline{\ell}_{iI})^{1/2} - L_i \tag{13}$$

where L_i is its neutral length.

The location of the origin of F_S relative to the origin of F_H is given by $\vec{D}$. Because F_S is fixed to the turntable, the direction of $\vec{D}$ is time varying while its length remains fixed. When $\psi_T = 0$, then

$$\vec{D} = \vec{D}_o \tag{14}$$

It follows that, in general,

$$\underline{D}_H = [d\cos(\psi_T + \gamma) \quad d\sin(\psi_T + \gamma) \quad D_{oz}]^T \tag{15}$$

where d, D_{oz}, and γ are constants.

TILT-COORDINATION

Consider a situation in which specific force at the origin of F_S is generated by tilt-coordination alone. Thus

$$\underline{f}_{SS} = -\underline{g}_S = -\underline{L}_{SI}\,\underline{g}_I \tag{16}$$

If ϕ_S and θ_S are assumed to be small angles, then Equation 16 can be approximated by

$$\underline{f}_{SS} = g\begin{bmatrix} \theta\cos\psi - \phi\sin\psi \\ -\theta\sin\psi - \phi\cos\psi \\ -1 \end{bmatrix}_S \tag{17}$$

Now, from work by Reid and Nahon (7) and Figure 3, the specific force to be simulated by tilt-coordination is given by the scaled, low-frequency part of the x- and y-components of $\underline{f}_{AA}$, represented by $\underline{fL}$, where

$$\underline{fL} = [fL_x \; fL_y]^T \tag{18}$$

Thus, from Equations 17 and 18 the tilt-coordination is given by

$$[\phi SL \quad \theta SL]^T = \underline{N}\,\underline{fL} \tag{19}$$

where

$$[\phi SL \quad \theta SL \quad 0]^T \equiv \underline{\beta SL} \tag{20}$$

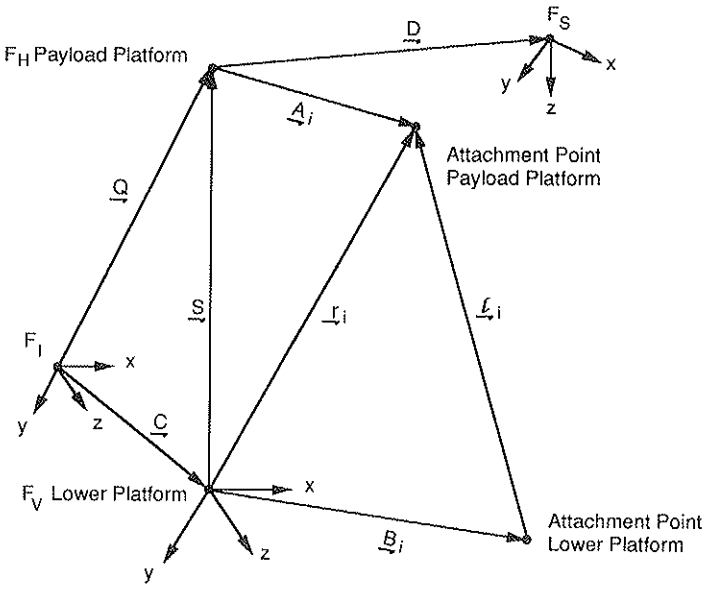

FIGURE 4 Vectors for a single actuator.

are the tilt-coordination Euler angles and

$$\underline{N} = g^{-1}\begin{bmatrix} -\sin\psi & -\cos\psi \\ \cos\psi & -\sin\psi \end{bmatrix}_S \tag{21}$$

In general, the tilt-coordination contribution to overall specific force is produced by adding $\underline{\beta SL}$ to that part of $\underline{\beta}_S$ produced by other effects as shown in Figure 3. Since tilt-coordination is intended to represent almost steady-state specific force, then it is important not to destroy the illusion by having the driver sense the angular velocity or tangential acceleration associated with the onset acceleration of the tilt. Software is included to place limits on both the tilt rate and the tilt acceleration used in tilt-coordination.

REVISED CLASSICAL WASHOUT

Referring to Equation 3 and Figure 3, $\underline{\beta}_S$ is made up of two parts:

$$\underline{\beta}_S = \underline{\beta 1HP} + \underline{\beta SL} \tag{22}$$

where $\underline{\beta 1HP}$ is the contribution due to $\underline{\omega}_{AA}$ and $\underline{\beta SL}$ the tilt-coordination. The path from $\underline{\omega}_{AA}$ to $\underline{\beta 1HP}$ follows standard classical washout practice (*7*). From Equations 7 and 22,

$$\underline{\omega}_{SS} = \underline{R}_S\,\dot{\underline{\beta}}_S = \underline{R}_S\,\mathrm{HPR}[\underline{T}_S\,\underline{\omega}'_{AA}] + \underline{R}_S\,\dot{\underline{\beta SL}} \tag{23}$$

where HPR[x] is the output of filter block HPR FILT for an input $x(t)$.

Equation 3 can now be used to determine ψ_T:

$$\psi_T = \psi_S - \psi_H \tag{24}$$

where ψ_S comes from Equation 22. Take

$$\psi_T = k_{T\psi_S} \tag{25}$$

$$\psi_H = (1 - k_T)_{\psi_S} \tag{26}$$

k_T is taken to be either unity or 0. When k_T is unity, all of ψ_S is generated by the turntable and none by the hexapod. When k_T is 0, all of ψ_S is generated by the hexapod and none by the turntable. Equations 25 and 26 are represented by the SPLIT block in Figure 3. Thus, from Equations 25 and 26,

$$\underline{\beta}_H = [\phi_S \quad \theta_S \quad (1 - k_T)_{\psi_S}]^T \tag{27}$$

In addition, a scaling factor k_{yr} has been included in order to allow ψ_T to be scaled up for special effects.

To generate $\underline{\omega}_{HH}$ and $\dot{\underline{\omega}}_{HH}$ for use in other sections of the algorithm, use

$$\underline{\omega}_{HH} = \underline{R}_H\,\dot{\underline{\beta}}_H \tag{28}$$

and its time derivative. Also define

$$\omega_T = \dot{\psi}_T \tag{29}$$

Next deal with the linear motion equations. Consider a Point P fixed to F_S and located relative to the origin of F_S by $\underline{OP}_S$ where

$$\underline{OP}_{SS} = [x' \quad y' \quad z']^T = \text{constant} \tag{30}$$

Let P be located relative to the origin of F_H by $\underline{OP}_H$ where

$$\underline{OP}_{HH} = [x \quad y \quad z]^T \tag{31}$$

Since $\underline{D}$ represents the location of the origin of F_S relative to F_H, it follows that

$$\underline{OP}_{HH} = \underline{D}_H + \underline{L}_{HS}\,\underline{OP}_{SS} \tag{32}$$

From Equations 6, 15, 30, 31, and 32

$$\underline{OP}_{HH} = \begin{bmatrix} d\cos(\psi_T + \gamma) + x'\cos\psi_T - y'\sin\psi_T \\ d\sin(\psi_T + \gamma) + x'\sin\psi_T + y'\cos\psi_T \\ D_{o_z} + z' \end{bmatrix} \tag{33}$$

$$\dot{\underline{OP}}_{HH} = \begin{bmatrix} -y\omega_T \\ x\omega_T \\ 0 \end{bmatrix} \tag{34}$$

$$\ddot{\underline{OP}}_{HH} = \begin{bmatrix} -y\dot{\omega}_T - x\omega_T^2 \\ x\dot{\omega}_T - y\omega_T^2 \\ 0 \end{bmatrix} \tag{35}$$

Since the classical washout algorithm attempts to match the vehicle's specific force at the origin of F_S, we will initially deal with the case where $\underline{OP}_{SS} = \underline{0}$. Following the development described by Reid and Grant (*6*) for the inertial acceleration of a point moving with respect to a translating and rotating frame, let the point be the origin of F_S and let F_H be the translating and rotating frame. It follows that

$$\underline{a}_{SH} = \underline{a}_{HH} + \underline{aa}_H \tag{36}$$

where

$\underline{a}_S$ = inertial acceleration of origin of F_S,
$\underline{a}_H$ = inertial acceleration of origin of F_H, and

$$\underline{aa}_H = \ddot{\underline{OP}}_{HH} + 2\underline{\Omega}_H\dot{\underline{OP}}_{HH} + [\underline{\Omega}_H\underline{\omega}_H + \dot{\underline{\omega}}_H]\underline{OP}_{HH} \tag{37}$$

where

$$\underline{OP}_{SS} = \underline{0}$$

$$\underline{\Omega}_H = \begin{bmatrix} 0 & -r & q \\ r & 0 & -p \\ -q & p & 0 \end{bmatrix}_{HH} \tag{38}$$

$$\underline{\omega}_{HH} = [p_{HH} \quad q_{HH} \quad r_{HH}]^T \tag{39}$$

Now from Equation 36

$$\underline{a}_{SI} = \underline{a}_{HI} + \underline{L}_{IH}\,\underline{aa}_H = \underline{a}_{HI} + \underline{aa}_I \tag{40}$$

Note that $\underline{a}_{II}$ is made up of the sum of the inertial acceleration of the x-y carriage and the acceleration of the hexpod frame F_H relative to the x-y carriage.

At this stage in the development, consider how the simulator acceleration command signals would be formed if there were no high-pass filtering of the linear motion commands (i.e., remove blocks HPS FILT and HPI FILT in Figure 2). Designate the variables altered by this lack of filtering by $(\tilde{})$. Thus Equation 40 becomes

$$\underline{\tilde{a}}_{SI} = \underline{\tilde{a}}_{II} + \underline{aa}_I \tag{41}$$

In classical washout it is attempted to make $\underline{f}_{SS}$ as similar to $\underline{f}'_{AA}$ as possible. In the absence of filtering take

$$\underline{\tilde{f}}_{SS} = \underline{f}'_{AA} \tag{42}$$

Thus

$$\underline{\tilde{a}}_{SS} = \underline{\tilde{f}}_{SS} + \underline{g}_S = \underline{f}'_{AA} + \underline{g}_S \tag{43}$$

and

$$\underline{\tilde{a}}_{SI} = \underline{L}_{IS}\,\underline{f}'_{AA} + \underline{g}_I \tag{44}$$

Thus, from Equations 41 and 44,

$$\underline{\tilde{a}}_{II} = \underline{L}_{IS}\,\underline{f}'_{AA} + \underline{g}_I - \underline{aa}_I \tag{45}$$

and $\underline{\tilde{a}}_{II}$ is the motion command signal to be sent to the hexapod and the x-y carriage. Let

$$\underline{\tilde{a2I}} = \underline{\tilde{a}}_{II} = \underline{L}_{IS}\,\underline{a2S} = \underline{L}_{IS}(\underline{f}'_{AA} + \underline{g}_S - \underline{aa}_S) \tag{46}$$

Now, to protect the hexapod and the x-y carriage, the signals $\underline{a2S}$ and $\underline{a2I}$ are passed through high-pass filters before being sent to the hardware. Because of the presence of the turntable, the orientation of the x- and y-axes of F_S with respect to those of F_I can vary without limit. Thus, the application of different degrees of filtering to the x- and y-components of $\underline{a2S}$ is best accomplished by filtering them in the F_S frame. In Figure 2 this is handled by the HPS FILT block (which leaves the z-component of $\underline{a2S}$ untouched). The result of this process is then expressed in F_I components by $\underline{a2I}$. As demonstrated elsewhere (*7*), high-pass filtering in F_S does not ensure that drifting and offsets will not occur in the simulator hardware. This requires high-pass filtering in the F_I frame. This is done by passing $\underline{a2I}$ through HPI FILT and then double integrating this filtered acceleration to produce the simulator displacement $\underline{Q}'_I$. It was also pointed out that filtering in F_I downstream of $\underline{L}_{IS}$ can lead to crosstalk among the $\underline{f}_{SS}$ components felt by the driver in the simulator (*7*). In the present case, with the possibility of large values for ψ_S, this can be a particular problem. To minimize these effects HPI FILT should be selected to be as mild as possible (i.e., select large values for natural frequency).

Initially the tilt-coordination crossfeed signal $\underline{f1}$ (see Figure 2) was formed from $(\underline{f}'_{AA} - \underline{aa}_S)$ in order to maximize the amount of $\underline{a2}$ sent through tilt-coordination. However, it was found that some of the high-frequency components in $\underline{aa}_S$ (due to $\underline{\dot{\Omega}}_H \underline{OP}_{IH}$) produced a destabilizing loop closure that could cause the algorithm to oscillate. This was corrected by allowing only the low-frequency part of $\underline{aa}_H$ to be used in tilt-coordination, namely $\underline{aa1}_H$, where

$$\underline{aa1}_H = [-x\omega_T^2 \quad -y\omega_T^2 \quad 0]^T \tag{47}$$

This was achieved by writing $\underline{a2S}$ as

$$\underline{a2S} = [\underline{f}'_{AA} - \underline{L}_{SH}(\underline{aa}_H - \underline{aa1}_H)] + \underline{g}_S - \underline{L}_{SH}\,\underline{aa1}_H \tag{48}$$

and arranging things as shown in Figure 2.

In Figure 2 $\underline{Q}'_I$ is the displacement command sent to the hexapod and the x-y carriage. To take full advantage of the simulator's design, the x- and y-components of $\underline{Q}'_I$ must be partitioned between the hexapod and the x-y carriage. It is assumed that the bandwidth of the hexapod is wider than that of the x-y carriage, thus it makes sense to base the partition on frequency content. This can be arranged to ensure that the largest displacements are carried out by the x-y carriage. Several alternatives were examined before the complementary filters approach was selected.

The block diagram of the complementary filters (LPC FILT) is included in Figure 2. They are applied to the x- and y-components of $\underline{Q}'_I$. The high-pass filters HPS FILT and HPI FILT are tuned to limit the low-frequency commands to the x-y carriage. The low-pass filter LPC FILT is tuned to send the high-frequency signals to the hexapod and the lower-frequency signals (which tend to produce large-amplitude motions) to the x-y carriage. The corresponding transfer functions for the x- and y-components are

$$\underline{\bar{C}}'_I = \underline{\overline{a2I}}\ [\text{HPI} \times \text{LPC}] \tag{49}$$

$$\underline{\bar{S}}'_I = \underline{\overline{a2I}}\ [\text{HPI}(1 - \text{LPC})] \tag{50}$$

and

$$\underline{\bar{Q}}'_I = \underline{\bar{C}}'_I + \underline{\bar{S}}'_I = \underline{\overline{a2I}}\,\frac{1}{s^2}\,\text{HPI} \tag{51}$$

In solving the differential equations corresponding to Equations 49 and 50, the initial conditions $\underline{C}'_I(0)$ and $\underline{S}'_I(0)$ are selected so as to start the simulator from a desired location. Usually this will be with all the actuators extended to half their stroke, although in special cases a bias toward some other location may be useful.

HARDWARE DRIVE SIGNALS

Although the scale factors, input limiters, and high-pass filters of the motion drive algorithm are intended to reduce the chances of the hardware's exceeding its limits, they cannot prevent this from happening for all system inputs. For this reason, software limiting is placed between the outputs from the washout algorithms and the hardware. For the hexapod and the x-y carriage, the limits are placed on displacement and velocity of the actuators. For the turntable, a limit is placed only on velocity. The limiting algorithm is fully described elsewhere (*8*). (The only addition has been the use of $\omega_b = 1/\Delta t$ in the velocity-limiting algorithm.) The limiting

blocks are shown at the output side of Figures 2 and 3. The drive signals including output limiting are ℓ_{3i} for the hexapod, $\underline{C}_I$ for the x-y carriage, and ψ_{TT} for the turntable.

INTERACTION BETWEEN TILT-COORDINATION AND TURNTABLE MOTION

The addition of the turntable creates the potential for unwanted ω_T interactions with tilt-coordination. Hence tuning of the motion-drive algorithm increases in complexity.

To demonstrate this interaction, consider Equation 23 for $\underline{\omega}_{SS}$. The term $\underline{R}_S\,\underline{\beta\dot{S}L}$ can contain unwanted contributions to $\underline{\omega}_{SS}$ representing false motion cues. From Equations 18 to 21 it follows that

$$\underline{\beta\dot{S}L} = \frac{1}{g}\begin{bmatrix} \sin\psi_S(fL_y\dot{\psi}_S - f\dot{L}_x) - \cos\psi_S(fL_x\dot{\psi}_S + f\dot{L}_y) \\ -\cos\psi_S(fL_y\dot{\psi}_S - f\dot{L}_x) - \sin\psi_S(fL_x\dot{\psi}_S + f\dot{L}_y) \\ 0 \end{bmatrix} \tag{52}$$

Assuming that tilt rates are small, $f\dot{L}_x$ and $f\dot{L}_y$ can be dropped into Equation 52, giving

$$\underline{\beta\dot{S}L} = \frac{\dot{\psi}_S}{g}\begin{bmatrix} -fL_x\cos\psi_S + fL_y\sin\psi_S \\ -fL_x\sin\psi_S - fL_y\cos\psi_S \\ 0 \end{bmatrix} \tag{53}$$

Thus, from Equations 9, 25, 29, and 53,

$$\underline{R_S\beta\dot{S}L} = \frac{\omega_T}{gk_T} \times \begin{bmatrix} -fL_x + (1-\cos\theta_S)(fL_x\cos^2\psi_S - fL_y\sin\psi_S\cos\psi_S) \\ -fL_y + (1-\cos\theta_S)(fL_y\sin^2\psi_S - fL_x\sin\psi_S\cos\psi_S) \\ \sin\theta_S(fL_y\sin\psi_S - fL_x\cos\psi_S) \end{bmatrix} \tag{54}$$

In Equation 54 it is seen that the products $\omega_T fL_x$ and $\omega_T fL_y$ appear as factors in every term. This is the undesired interaction because it leads to false cues in $\underline{\omega}_{SS}$ that could be sensed by the driver in the simulator.

COMPUTER-BASED SIMULATOR TESTS

To assess the capabilities of the proposed motion algorithm and hardware configuration, a computer simulation was carried out for a number of typical driving maneuvers. In these tests the size of the simulator was fixed with the hexapod actuators having a stroke of ± 0.67 m about 0 and the x-y carriage having the same ± 13.72 m travel in both directions about 0. In all cases the motion algorithm parameters were selected to produce representative system response. (The evaluation of simulator motion performance made hereupon is based on the authors' experience with simulator motion.) The car response data were produced by specifying the inputs to a simple vehicle model representing a 1814-kg car as documented by Reid and Grant (*9*).

Entry and Steady Turn Maneuvers

The entry and steady turn maneuver was entered at 60 km/hr, and the car's trajectory was a circle of 150-m radius. This was a fairly mild turn, generating about 0.25 g of side force on the driver (see Figure 5). Three simulator configurations were tested for this particular maneuver, designated as EST1, EST2, and EST3.

In EST1 all the simulator motion subsystems were active. The simulator x-y carriage displacement and turntable angle are shown in Figure 6. The displacement shown in this plot is significantly different from that for the car because of the high-pass filters and the use of tilt-coordination to represent sustained lateral specific force. Figure 5 gives plots of the driver's lateral specific force in the cab frame for the car and the simulator. The simulator does a good job of representing this motion cue with a rapid onset at the beginning and the correct steady-state value. The small dip in specific force in the simulator following the onset cue is due to tilt-coordination limiting the buildup of the tilt-coordination cue. The initial simulator specific force cue does not reach the car's initial value because of the overall filtering action of the motion algorithm. Figure 7 shows the car's sustained yaw rate and the washed-out yaw rate of EST1. Because of the high-pass nature of the human vestibular system, however, the yaw rates sensed by the driver in these two cases are quite similar.

In EST2 the yaw component of HPR FILT (see Figure 3) has been deleted (opened up) with the remainder of the simulator configuration kept the same as EST1. The simulator trajectory is shown in Figure 6. Under these conditions the simulator approaches a steady-state yaw rate as shown in Figure 7. Note the oscillatory nature of the simulator's yaw rate response. This is an example of the interaction between tilt-coordination and turntable motion given by Equation 54. The corresponding tilt-coordination angles will also be oscillatory in order to produce a constant specific force on the driver in the cab frame (see Figure 5).

In EST3 the turntable has been turned off and the hexapod is used to produce all yawing effects. The high-pass filters have been tuned to take this change into account. As shown in Figure 6 the x-y carriage displacement is now primarily a lateral displacement although a small longitudinal displacement is present. From Figure 7 it can be seen that the yaw rate cue is of very short duration, being primarily an onset cue. This results in a sensed yaw rate that is significantly different from that produced by the car. The lateral

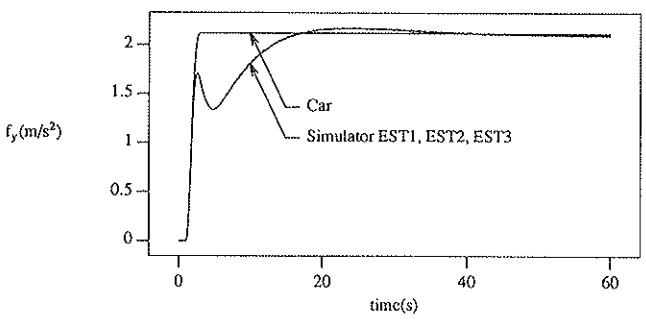

FIGURE 5 Driver's lateral specific force in cab frame for entry and steady turn.

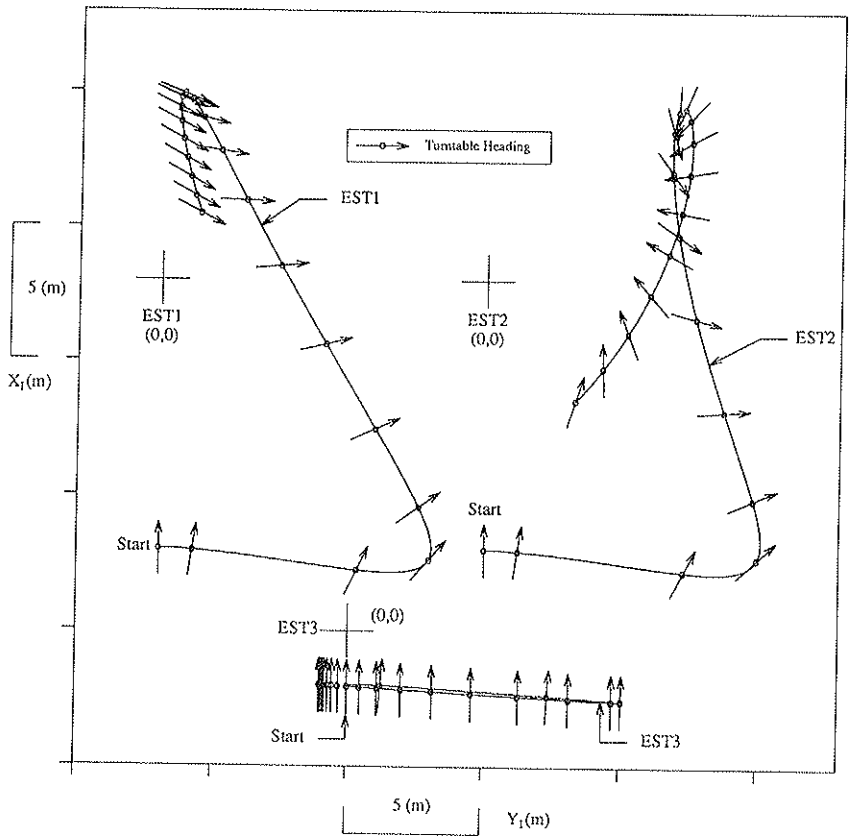

FIGURE 6 Simulator trajectories for EST1, EST2, and EST3.

specific force is unchanged from EST1 and EST2 as shown in Figure 5.

Braking Maneuver

The braking maneuver (BRK) was moderate (0.25 *g*) and began from a steady forward speed of 80 km/hr. All the simulator subsystems were active. The resulting driver's longitudinal specific force in the cab frame is shown in Figure 8 for both the car and the simulator. The simulator produces a good onset cue followed by a sag in specific force due to tilt-coordination limiting. There is a good f_x transient cue when the car comes to a full stop followed by a large false cue caused by tilt-coordination limiting, which restricts the rapidity with which the tilt-generated specific force can be removed. This braking maneuver used up 21 m of *x-y* carriage travel.

Single Lane Change

The single lane change (with a maximum lateral acceleration of approximately 0.125 *g*) was entered from 60 km/hr. Two simulator configurations were tested for this maneuver, and they were designated as LC1 and LC2.

In LC1 all the simulator motion subsystems were active. This case represents an attempt to minimize the amount of filtering and tilt-coordination in order to take full advantage of the large displcements of the simulator. This resulted in as

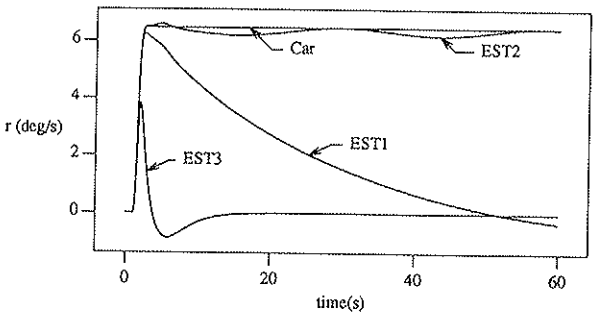

FIGURE 7 Yaw rate for entry and steady turn.

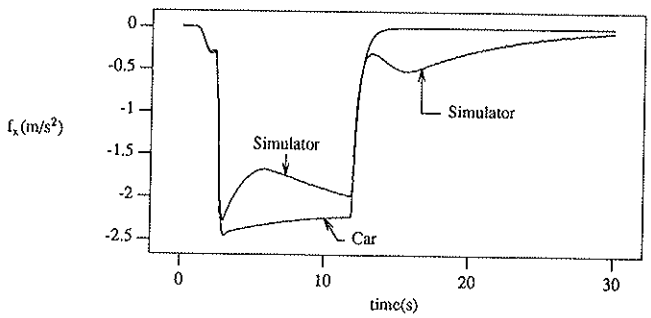

FIGURE 8 Longitudinal specific force for braking maneuver.

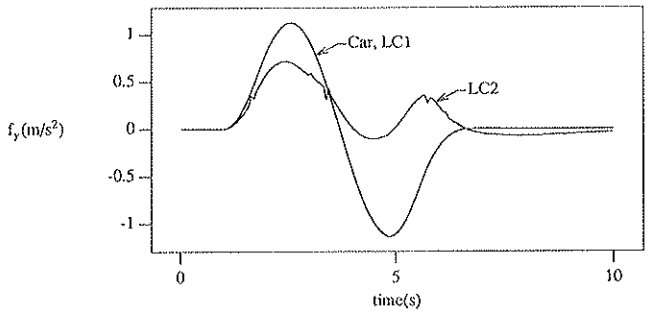

FIGURE 9 Driver's lateral specific force in cab frame for single lane change maneuver.

close to direct duplication of the car's motion as was possible. Only mild high-pass filtering in the x- and z-channels remained. Tilt coordination and filtering of the angular degrees of freedom were eliminated. The resulting simulator trajectory used about the same lateral travel as the actual car (approximately 4 m). It was primarily a lateral motion with a very small amount of longitudinal motion. The simulation of $\underrightarrow{f}$ and $\underrightarrow{\omega}$ in the cab frame for the driver was almost perfect (see Figure 9 for $\underrightarrow{f}$).

In LC2 the turntable and the x-y carriage were turned off. The amount of filtering was increased and the tilt-coordination turned back on. All of the yawing motion is provided by the hexapod. From Figure 9 it can be seen that this has resulted in a degraded simulator specific force cue. This is primarily the result of turning off the x-y carriage. The simulator yaw rate still duplicated that of the car because the maneuver is sufficiently limited in yaw displacement that the hexapod can handle it with no trouble.

SUMMARY

A computer simulation has been developed that can be used to study the performance and specifications of large-amplitude motion-bases intended for driving simulator applications. Both the motion drive algorithm and the physical motion of the simulator are modeled. The simulator configuration selected for study consisted of an unrestricted turntable on top of a hexapod motion platform supported by a large-amplitude x-y carriage.

Algorithms have been selected that divide the motion among the three major subsystems. The commands sent to the x-y carriage are based on their frequency content while those sent to the turntable are often selected to reduce the hexapod motion commands to 5 degrees of freedom.

A tilt-coordination algorithm has been developed that accounts for the presence of the turntable. In addition, an unavoidable interaction between tilt coordination and turntable angular velocity has been identified.

The testing of the motion algorithm on several common car maneuvers has highlighted the benefits possible from the proposed simulator configuration. The large-amplitude x-y carriage can be used to generate excellent specific force cues while minimizing the need for tilt-coordination in certain cases. The turntable provides excellent yaw rate cues.

ACKNOWLEDGMENTS

The work described in this paper was sponsored by the Transportation Research Center (TRC), in support of a contract with NHTSA.

REFERENCES

1. J. Drosdol and F. Panik. *The Daimler-Benz Driving Simulator. A Tool for Vehicle Development*. SAE Paper 850334. International Congress and Exposition, Detroit, Mich., 1985.
2. S. Nordmark, H. Jansson, M. Lidstrom, and G. Palmkvist. A Moving Base Driving Simulator with Wide Angle Visual System. Presented at 64th Annual Meeting of the Transportation Research Board, Washington, D.C., Jan. 1985.
3. Y. Gutman and M. Filshtinsky. *Motion Analysis of a Driving Simulator with Nine Degrees-of-Freedom*. Evans and Sutherland Computer Corp., Salt Lake City, Utah, 1987.
4. *Proc., Ford Motor Company Symposium on Driving Simulation*. Dearborn, Mich., Nov. 1990.
5. L. D. Reid and P. R. Grant. *Motion-Base Development Package for NADS*. Transportation Research Center for Ohio, East Liberty, 1991.
6. L. D. Reid and P. R. Grant. *Motion-Base Development Package for NADS. Part 2: Including the Turntable*. Transportation Research Center of Ohio, East Liberty, 1992.
7. L. D. Reid and M. A. Nahon. *Flight Simulation Motion-Base Drive Algorithms: Part 1—Developing and Testing the Equations*. UTIAS Report 296. University of Toronto Institute for Aerospace Studies, Downsview, Ontario, Canada, 1985.
8. L. D. Reid and M. A. Nahon. *Flight Simulation Motion-Base Drive Algorithms: Part 2—Selecting the System Parameters*. UTIAS Report 307. University of Toronto Institute for Aerospace Studies, Downsview, Ontario, Canada, 1986.
9. L. D. Reid and P. R. Grant. *A Preliminary Assessment of the Influence of Codetron on Car Driver Performance*. UTIAS Contract Report. University of Toronto Institute for Aerospace Studies, Downsview, Ontario, Canada, 1988.

APPENDIX
Notation

s = Laplace variable
Δt = computer step size
ωB = angular velocity of frame F_B with respect to frame F_I
$\underrightarrow{(\ )}$ = vector
$\underline{b}_B$ = components of $\underrightarrow{b}$ expressed in frame F_B (a three-element column matrix)
$\underline{B}$ = matrix
$\underline{B}_T$ = transpose of $\underline{B}$
$(\ )_B$ = variables related to frame F_B
$\dot{x} = \frac{dx}{dt}$
$\bar{x}$ = Laplace transform of $x(t)$

The discussions and conclusions in this paper represent the opinions of the authors and not necessarily those of the TRC or NHTSA.

Publication of this paper sponsored by Committee on Simulation and Measurement of Vehicle and Operator Performance.